

Carrier capture by threading dislocations in (In,Ga)N/GaN heteroepitaxial layers

U. Jahn,* O. Brandt, and E. Luna

Paul-Drude-Institut für Festkörperelektronik, Hausvogteiplatz 5-7, 10117 Berlin, Germany

X. Sun, H. Wang, and D. S. Jiang

Institute of Semiconductors, Chinese Academy of Sciences, Beijing, China

L. F. Bian and H. Yang

Suzhou Institute of Nano-Tech and Nano-Bionics, Chinese Academy of Sciences, Suzhou, China

(Received 24 November 2009; revised manuscript received 3 February 2010; published 12 March 2010)

Using spatially resolved cathodoluminescence spectroscopy, we investigate the spatial luminescence distribution in a fully strained (In,Ga)N layer, in particular, its correlation with the distribution of threading dislocations (TDs). Regarding the impact of TDs on the luminescence properties, we can clearly distinguish between pure edge-type TDs and TDs with screw component. At the positions of both types of TDs, we establish nonradiative recombination sinks. The radius for carrier capture is at least four times larger for TDs with screw component as for pure edge-type TDs. The large capture radius of the former is due to a spiral-like growth mode resulting in an increase in the In content in the center of the spiral domains in comparison to their periphery.

DOI: [10.1103/PhysRevB.81.125314](https://doi.org/10.1103/PhysRevB.81.125314)

PACS number(s): 78.66.Fd, 78.67.-n, 78.55.Cr, 78.60.Hk

A decade ago, Heying *et al.*¹ reported on dislocation mediated surface morphologies of GaN grown by molecular-beam epitaxy and metal-organic chemical-vapor deposition (MOCVD) on sapphire substrates. According to their report, the step-flow surface morphology of GaN is modified mainly by screw (α -type) and mixed (β -type) dislocations. Pure edge dislocations (γ -type) do not have any essential influence on the growth mode. Threading dislocations (TDs) with screw component (α - or β -type) lead to pinned steps during step-flow growth, which in turn can result in a modified step flow, namely, spiral growth, in particular, for conditions far away from equilibrium. This is, for example, the case for the MOCVD growth of (In,Ga)N, where the growth temperature (T_G) has to be low (around 700 °C in comparison to 1050 °C for GaN) to suppress In desorption. Thus, the surface morphology of (In,Ga)N layers is often dominated by spiral-like hillocks.^{2,3}

Moreover, α - or β -type TDs act as seeds for the formation of so-called V-pit defects, which is even enhanced for the growth of (In,Ga)N by segregation of In on (10.1) facets of the inverted pyramids of V-pits.^{4,5} The impact of the spiral-like growth as well as of the TDs on the luminescence distribution of (In,Ga)N-related layers has mostly been investigated for (In,Ga)N/GaN quantum-well structures,^{6,7} where, however, the luminescence properties are influenced by additional effects such as thickness fluctuations including interface roughness and the quantum-confined Stark effect. For thick (In,Ga)N films, such investigations have been performed indirectly by Sato *et al.*⁸ by comparing (In,Ga)N layers grown on sapphire with layers grown on GaN substrates. Since the (In,Ga)N layers grown on sapphire, which exhibited much higher TD densities, showed more severe variations in the In content than those grown on GaN, it has been inferred that the In-content fluctuations are mediated by TDs.

In this paper, we show directly the impact of TDs originating from a GaN/sapphire substrate on the surface morphology and lateral luminescence distribution of a 50-nm-

thick (In,Ga)N layer grown by MOCVD. The impact of pure edge-type TDs and TDs with screw component can be distinguished and is discussed in detail. The (In,Ga)N layer under investigation is fully strained, thus preventing the formation of relaxation-related defects and hence any influence on the results discussed here.

The structure was grown in a vertical Thomas Swan MOCVD system. Prior to growth, the substrate was thermally cleaned at 1060 °C for 400 s in a hydrogen atmosphere. The layer sequence started with a 20-nm-thick and 3- μ m-thick low-temperature GaN nucleation and GaN buffer layer, respectively, followed by the (In,Ga)N layer. As precursors, we used trimethylindium (TMIn), trimethylgallium (TMGa), and ammonia (NH₃). For the growth of GaN and (In,Ga)N, H₂ and N₂ were used as carrier gas, respectively. The growth temperature T_G amounted to 530 °C and 1040 °C for the GaN nucleation and buffer layer, respectively, and 680 °C for the (In,Ga)N layer. The nominal thickness of the latter was chosen to be 50 nm.

The lateral luminescence distribution of the (In,Ga)N/GaN layers was investigated by spectrally and spatially resolved cathodoluminescence (CL) in a field-emission gun scanning electron microscope (SEM), where the surface morphology can be imaged by means of secondary electrons (SEs) simultaneously with the monochromatic CL intensity distribution. The CL/SE experiments have been performed using a SEM ULTRA55 equipped with a Gatan monoCL3 and He-cooling stage system allowing for sample temperatures between 6 and 300 K. For the acquisition of both CL spectra and CL images, the acceleration voltage of the electron beam was chosen to be 5 kV, which on the one hand, ensures that an essential portion of the beam energy is deposited within the thin (In,Ga)N layer and that on the other hand, the upper part of the GaN buffer layer is still directly excited. In this way, a CL signal can be obtained from both layers at the same time. The beam current was chosen to be 0.2 and 1 nA for CL measurements (imaging, spectra acqui-

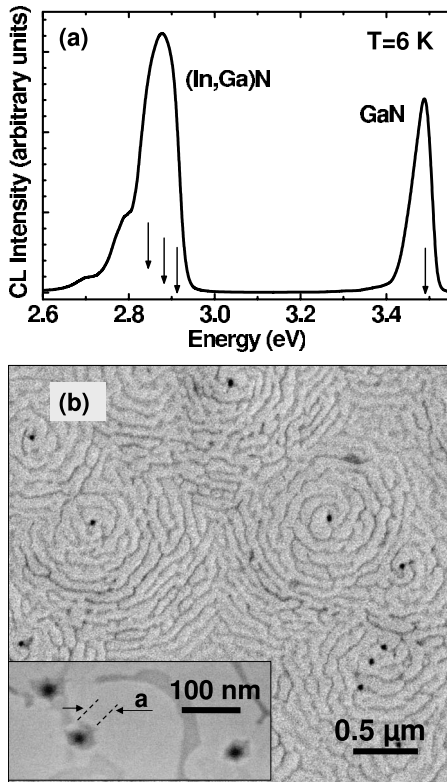


FIG. 1. (a) Normalized CL spectrum averaged over an area of about $20 \times 20 \mu\text{m}^2$ of the (In,Ga)N/GaN heteroepitaxial layer structure at 6 K. The arrows point to the energies corresponding to the CL images in Figs. 4(a) and 4(c)–4(e). (b) SEM surface image of the (In,Ga)N/GaN sample. Inset: magnified SEM image showing V-pit defects. a marks the base length of the V-pit hexagon.

sition) at 6 K and 300 K, respectively. Throughout all the CL experiments, the spectral resolution amounted to 1.4 nm corresponding to a slit width of the CL spectrometer of 0.5 nm.

Transmission electron microscopy (TEM) has been performed using a Jeol JEM 3010 microscope operating at 300 kV. The plan-view specimens were prepared by mechanical polishing from the substrate backside followed by Ar-ion milling. X-ray diffraction (XRD) was performed with a Philips X’Pert PRO™ four-circle diffractometer equipped with a Cu $K\alpha 1$ source in the focus of a multilayer x-ray mirror, a Ge(022) hybrid monochromator, and a three-bounce Ge(022) analyzer. Both symmetric ω - 2θ scans across the (002) reflection and reciprocal space maps around the asymmetric (105) reflection were recorded in triple-axis configuration.

Figure 1(a) shows a CL spectrum of the (In,Ga)N/GaN heteroepitaxial layer structure acquired at a sample temperature of 6 K. The excitation was averaged over an area of about $20 \times 20 \mu\text{m}^2$. The spectrum consists of two lines, where the one centered at 3.488 and 2.885 eV represents the donor-bound exciton transition of the GaN template layer and the optical near-band-gap transition of the (In,Ga)N layer, respectively. The full width at half maximum (FWHM) of the (In,Ga)N-related spectrum amounts to about 90 meV. Moreover, it exhibits two shoulders on the low-energy side, stemming from longitudinal optical-phonon replicas of the main line of the spectrum as inferred from their energy separation

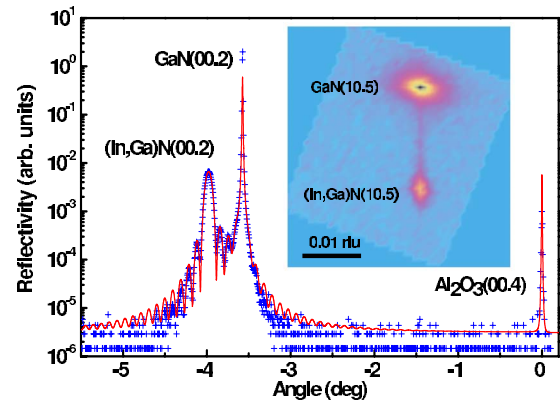


FIG. 2. (Color online) ω - 2θ XRD scan across the GaN(00,2) reflection of the (In,Ga)N/GaN sample. The symbols and line represent the experimental data and numerical simulation, respectively. The inset shows a reciprocal space map around the asymmetric (10,5) reflection of the same sample.

of about 90 meV. The surface structure of the sample is represented in Fig. 1(b) showing a SE image of the (In,Ga)N layer. The surface exhibits a spiral-like morphology, with at least one V-pit defect being situated in the center of each spiral as shown in the inset of Fig. 1(b). The basis length (a) of the hexagon of these V pits amounts to about 30 nm. According to the relation $d=1.63a$ between the depth d and a of a V-pit,⁴ this defect is initiated near the (In,Ga)N/GaN interface. Since it is known that both the evolution of V-pit defects and a spiral-like growth mode is triggered by α - or β -type TDs,^{4,9} it is obvious that this kind of extended defects exhibits a large influence on the growth of at least thin (In,Ga)N layers.

In order to determine the strain state and composition of the layer, we performed XRD experiments. The inset of Fig. 2 shows the reciprocal space map of the (In,Ga)N/GaN layer structure, which indicates that this layer is fully strained (1.6% misfit) with a relaxation degree $R=0$. Using this result, we determine the In content x of this layer by fitting the ω - 2θ scan of Fig. 2 yielding $x=0.147$. As a second result of the above fit, we determine the layer thickness d to amount to 48 nm, which is confirmed by SE imaging of the cleaved edge of the sample. From these experimental results, we conclude that (In,Ga)N layers with a thickness-strain product of less than $750 \text{ \AA}\%$ remain pseudomorphic. Extended defects in the layer are thus exclusively due to the GaN template.

TEM is the method of choice to directly determine the character of dislocations and their distribution in thin films. Follstaedt *et al.*¹⁰ proposed a procedure that enables the detection and identification of all vertical TD types (edge, screw, and mixed) in (0001) nitride layers from a single plan-view micrograph. This is possible because, in addition to the so-called “ $\mathbf{g} \cdot \mathbf{b}$ ” contrast criterion (which evaluates the alignment of the strain field of the dislocation with Burgers vector \mathbf{b} with respect to the diffraction vector \mathbf{g} producing the image contrast), a second contrast mechanism due to strain relaxation of screw dislocations at the free surface operates. In the plan-view micrograph of Fig. 3, the specimen is tilt about 18° off the $[0001]$ zone axis to obtain two-beam conditions with $\mathbf{b}=[1\bar{1}20]$. Three types of TDs can clearly be distin-

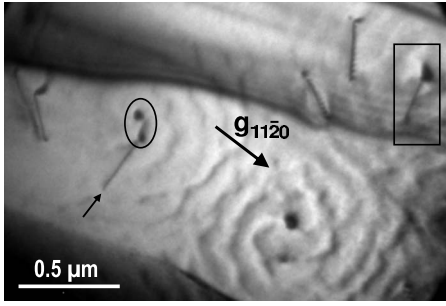


FIG. 3. Plan-view transmission electron microscope image of the (In,Ga)N/GaN sample obtained for $\mathbf{b}=[11\bar{2}0]$ with the specimen tilted by about 18° off the $[0001]$ zone axis. The circle indicates a screw TD, the box a mixed TD, and the arrow an edge TD.

guished: (i) pure screw TDs, i.e., α -type. In this case, the outcrops of screw dislocations are reflected by pairs of isolated spots (circled). (ii) Mixed TDs, i.e., β -type, where the pair of spots are connected by a line in between them (boxed). (iii) Pure edge TDs, i.e., γ -type, which are observed as lines (arrow). Independently of the type, the estimated TD density in the sample amounts to about $4 \times 10^8 \text{ cm}^{-2}$. The ratio between α - plus β -type and γ -type TDs amounts to about 0.5. Moreover, outcrops of screw and mixed dislocations are observed at the center of regions with a spiral-like corrugated surface morphology. Another important result of the TEM investigation is that relaxation-related extended defects could not be observed. For (In,Ga)N/GaN heteroepitaxial layers, Jahnen *et al.*¹¹ and Liu *et al.*¹² observed the evolution of relaxation-related dislocation loops at the (In,Ga)N/GaN interface initiated at the apex and side facets of V-pit defects, respectively. Even such a local plastic relaxation has not been observed within the immediate neighborhood of α - and β -TDs of the present (In,Ga)N/GaN layer structure.

Figure 4 shows CL images for various values of the CL detection energy E_{CL} and the SE image of the same region of the (In,Ga)N/GaN structure. In the CL image of Fig. 4(a) obtained at $E_{\text{CL}}=3.488 \text{ eV}$ (donor-bound exciton of GaN), the dark spots represent the TDs of the GaN template layer. About $\frac{1}{3}$ of the number of these TDs [marked by arrows in Fig. 4(a)] correlate with the appearance of V-pits of the SE

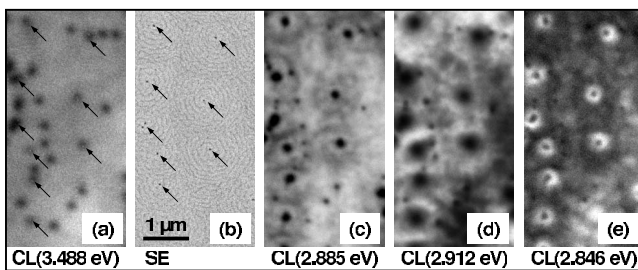


FIG. 4. (a), (c)–(e) CL and (b) SE images of the same region of the (In,Ga)N/GaN sample. The images have been acquired at 6 K. For the CL images, the detection energy E_{CL} is (a) near-band gap of GaN (3.488 eV), (c) at the center (2.885 eV), (d) on the high-energy (2.912 eV), and (e) on the low-energy side (2.846 eV) of the (In,Ga)N line as indicated by arrows in Fig. 1.

image shown in Fig. 4(b). Thus, dark spots marked by arrows in Fig. 4(a) are related to α - or β -type TDs, which typically initiate a spiral-like growth and the formation of V-pits.^{4,13} In Figs. 4(c)–4(e), we compare the CL images for values of E_{CL} corresponding to the center, the high-energy, and the low-energy side, respectively, of the (In,Ga)N CL spectrum [cf. arrows in Fig. 1(a)]. The CL intensity distribution varies significantly with the detection energy indicating lateral fluctuations of the optical transition energy on a micrometer scale. These fluctuations are clearly correlated with the V-pit and spiral domain distribution. In contrast, TDs which are not associated with V-pits and do not show any other detectable surface features, appear merely as small dark spots in these maps regardless of the value of E_{CL} . Furthermore, they do not influence the CL distribution in their neighborhood. We thus assign these small dark spots to γ -type TDs.

As expected from the XRD and TEM results shown above, there is a one-to-one correspondence between the total number of dark spots of the CL images obtained from the GaN template ($E_{\text{CL}}=3.488 \text{ eV}$) and from the epitaxially grown (In,Ga)N layer ($E_{\text{CL}}=2.885, 2.912, \text{ or } 2.846 \text{ eV}$). This number corresponds to a density of TDs of $3 \times 10^8 \text{ cm}^{-2}$. The ratio between the dark spots, which we assign to α - or β -type TDs and the ones assigned to γ -type TDs amounts to about 0.5. Both values (density and ratio) agree very well with the corresponding numbers found by TEM confirming the assignment of the dark spots of the CL images to the respective kind of TD. The impact of α - or β -type TDs on the one hand and γ -type TDs on the other hand on the luminescence distribution and morphology of the (In,Ga)N layer can be clearly distinguished. Comparing the CL images of Figs. 4(c) and 4(d) with the one of Fig. 4(e), we see that the intensity distributions of Figs. 4(d) and 4(e) show complementary contrasts except the centers of the TDs, which are darkly independent of the chosen value of E_{CL} indicating nonradiative recombination at this position. The immediate surroundings of the α - or β -type TDs represent low-energy regions (high intensity at $E_{\text{CL}}=2.846 \text{ eV}$) whereas the regions further away from the immediate surroundings of these defects represent high-energy regions (high intensity at $E_{\text{CL}}=2.912 \text{ eV}$).

The corresponding distribution of the near-band-gap energy of the (In,Ga)N layer is shown in more detail in Fig. 5. This figure represents the peak energy of CL spectra acquired along a line as a function of the scan position. The corresponding path way of the line scan, which is indicated by a white dashed arrow in the inset of Fig. 5, crosses two spiral domains with their V-pit defects being situated in the center of these domains. The resulting profile of the near-band-gap energy is characterized by minima at the positions of the V-pit defects and by energy barriers (maxima) at the periphery of the spiral domains. Such an energy profile can be explained by assuming that an accumulation of the In content in the center of the spiral domain is accompanied by a depletion of In within the periphery regions of the corresponding domains. Other possible origins for the occurrence of energy minima in conjunction with TDs or V-pit defects could be related to strain interaction or relaxation, respectively. However, an interaction of the layer strain with the strain field of

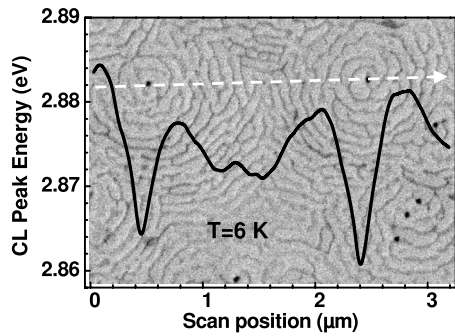


FIG. 5. Peak energy of CL spectra acquired along a line crossing two α - or β -type TDs at 6 K. Inset: SE image of the (In,Ga)N layer. The white arrow indicates the path way of the CL line scan.

the TDs cannot account for the observed energy minima since the α - or β -type TDs are terminated at the GaN/(In,Ga)N interface at the apex of the corresponding V-pit defects. Local plastic relaxation of the strain by means of the evolution of dislocation loops at the apex of the V-pit defects, which could lead to 130 meV deep energy minima,¹⁴ does obviously not occur since we could not find any relaxation-related defects by TEM. Elastic strain relaxation could occur via the side facets of the V pits, for which, however, one would expect a continuous decrease in the energy from the periphery toward the center of the V-pit. Thus, the observed distribution of the near-band-gap energy is rather a signature of a redistribution of In (material transport) during the growth than a result of a local strain relaxation related to the α - or β -type TDs and their V-pit defects.

The difference between α - or β -type TDs on the one hand and γ -type TDs on the other hand with regard to their influ-

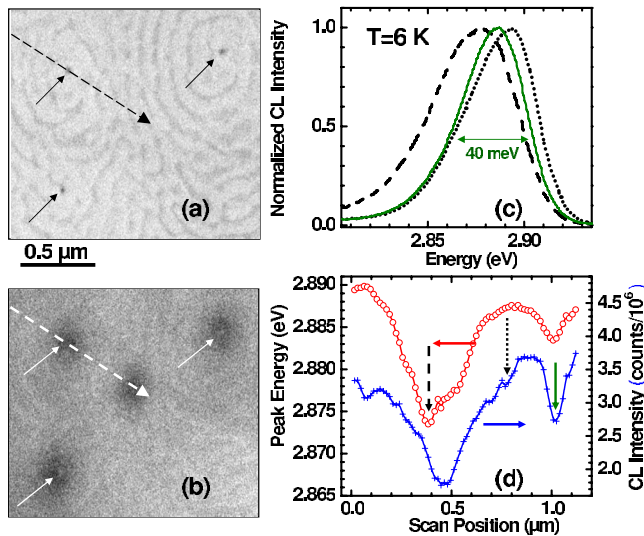


FIG. 6. (Color online) (a) SE and (b) CL image ($E_{CL}=3.488$ eV) of the (In,Ga)N/GaN heteroepitaxial layer structure. (c) Normalized CL spectra for the line scan marked by the dashed line in the images for the scan positions as indicated by vertical arrows in (d). (d) Peak energies (circles) and integrated CL intensities (crosses) of all spectra along the indicated path as a function of scan position. The SE and CL image as well as the CL spectra line scan have been acquired at 6 K.

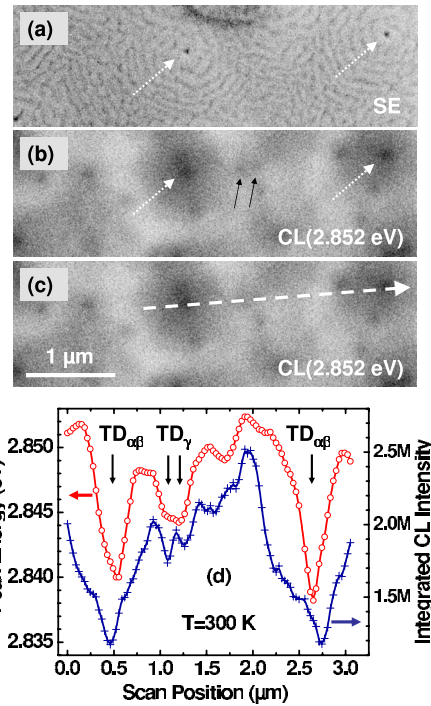


FIG. 7. (Color online) (a) SE, (b) and (c) CL image ($E_{CL}=2.852$ eV) of the same sample as in Fig. 6. (d) Peak energies (circles) and integrated CL intensities (crosses) as a function of scan position. In (a) and (b), the white dotted arrows indicate the position of the α - or β -type TDs. In (b), the black arrows indicate the positions of the γ -type TDs. The CL line scan data depicted in (d) have been acquired along the path way indicated by the dashed arrow in (c).

ence on the optical properties of the (In,Ga)N layers is studied in detail by means of CL line scans as represented in Fig. 6. The SE image of Fig. 6(a) shows three spirals with corresponding V-pits indicating the positions of three α - or β -type TDs intersecting the surface. In Fig. 6(b), the CL image of the same region obtained for $E_{CL}=3.488$ eV (donor-bound exciton of the GaN template layer) shows four dark spots, where three of them can be assigned to the V-pit positions of Fig. 6(a). The fourth one, which exhibits no feature at the surface of the layer, is assigned to a γ -type TD. CL spectra have been acquired along the path marked by the dashed line in Figs. 6(a) and 6(b). Following this line from left to right, the electron beam subsequently intersects the positions of an α - or β - and a γ -type TD.

Figure 6(c) shows three CL spectra acquired by spot excitation at the scan positions marked by the vertical arrows in Fig. 6(d). The FWHM of these spectra varies between 40 and 55 meV, which is still broad but much narrower than the one obtained for a large excitation area as shown in Fig. 1(a). This result visualizes the inhomogeneous spectral broadening of (In,Ga)N due to local variations in x on a micrometer scale. Despite the large FWHM, the spectral shift as a function of the scan position can clearly be recognized. Figure 6(d) represents the peak energies (circles) and integrated CL intensities (crosses) of all spectra obtained at 6 K along the path indicated. Let us emphasize the following features of this line scan: (i) both the CL peak energy (E_T) and the inte-

grated intensity (I_{CL}) exhibit minima at the positions of each kind of TDs. (ii) For the α - or β -type TD, the width of the minima are about four times larger than the one for the γ -type TD. (iii) The width of the latter is on the same order as the spatial resolution of CL (50–100 nm).

The minima of I_{CL} demonstrate the nonradiative character for both kinds of TDs. For the γ -type TD, the actual depth and width of the I_{CL} minimum are determined by the spatial resolution of the CL method and do not reflect the actual intensity drop and carrier capture radius (σ_γ) of the γ -type TD.^{15,16} Consequently, σ_γ is probably much smaller than the width of the measured CL intensity minimum. Since the width of I_{CL} of the α - or β -type TD is larger than the spatial resolution of the CL method, we can roughly estimate the exciton capture radius ($\sigma_{\alpha,\beta}$) to be on the order of a few hundred nanometers. This large value for $\sigma_{\alpha,\beta}$ is likely a result of the compositional gradient caused by these dislocations.

Figure 7 shows results of a CL line scan on the same sample as for Fig. 6 but performed at room temperature (RT). The SE image of Fig. 7(a) and the CL images of Figs. 7(b) and 7(c) represent the same region of the sample at RT. The white dotted and black arrows indicate the positions of α - or β -type and γ -type TDs, respectively. Consequently, the path way of the line scan, which is marked by a dashed arrow in Fig. 7(c), intersects two α - or β -type TDs and two γ -type TDs. Figure 7(d) represents the peak energies (circles) and integrated CL intensities (crosses) along the dashed line of Fig. 7(c). As for low temperatures, the CL intensity exhibits broad and deep minima for α - or β - and very narrow minima

for γ -type TDs. The intensity profiles of the former show a funnel-like shape and are broader than the corresponding intensity and energy distributions obtained at low T , indicating a larger influence of carrier diffusion on carrier capture at RT. Thus, the dominant contribution of α - or β -type TDs to nonradiative recombination in (In,Ga)N layers is even enhanced at RT. Consequently, a reduction in the density of α - or β -type TDs can result in a significant improvement of the quantum efficiency of heteroepitaxially grown (In,Ga)N layers, which is particularly important for the application of this materials system in photovoltaic devices. For the growth of (In,Ga)N/GaN QWs, the carrier capture by α - or β -type TDs can be blocked due to the evolution of thin sidewall QWs at the facets of V-pit defects, which are formed at the apex of these TDs.¹⁷ Since TDs with screw component provide obviously the main contribution to nonradiative recombination, the evolution of sidewall QWs surrounding these TDs and building effective energy barriers for carriers leads to an essential increase in the quantum efficiency of, for example, light-emitting diodes on the basis of (In,Ga)N/GaN QWs.

In conclusion, 50-nm-thick (In,Ga)N layers with an In content of 0.15 grown on a GaN template are fully strained and inherit all TDs from the template. Nonradiative recombination is observed at the positions of both of TDs regardless of their type. The carrier capture radius for nonradiative recombination is, however, at least four times larger for α - or β -type TDs compared to the one of γ -type TDs. This large capture radius of TDs with screw component is attributed to an enhanced In incorporation close to the core of the TDs.

*ujahn@pdi-berlin.de

¹B. Heying, E. J. Tarsa, C. R. Elsass, P. Fini, S. P. DenBaars, and J. S. Speck, *J. Appl. Phys.* **85**, 6470 (1999).

²S. Keller, B. P. Keller, M. S. Minsky, J. E. Bowers, U. K. Mishra, S. P. DenBaars, and W. Seifert, *J. Cryst. Growth* **189-190**, 29 (1998).

³R. A. Oliver, M. J. Kappers, and C. J. Humphreys, *J. Appl. Phys.* **97**, 013707 (2005).

⁴J. E. Northrup, L. T. Romano, and J. Neugebauer, *Appl. Phys. Lett.* **74**, 2319 (1999).

⁵L. T. Song, *J. Appl. Phys.* **98**, 084906 (2005).

⁶T. Sugahara, M. Hao, T. Wang, D. Nakagawa, Y. Naoi, K. Nishino, and S. Sakai, *Jpn. J. Appl. Phys., Part 2* **37**, L1195 (1998).

⁷A. Kaneta, M. Funato, Y. Narukawa, T. Mukai, and Y. Kawakami, *Phys. Status Solidi C* **3**, 1897 (2006).

⁸H. Sato, T. Sugahara, Y. Naoi, and S. Sakai, *Jpn. J. Appl. Phys., Part 1* **37**, 2013 (1998).

⁹J. Wu, W. Walukiewicz, K. M. Yu, W. Shan, J. W. Ager, E. E.

Haller, H. Lu, W. J. Schaff, W. K. Metzger, and S. Kurtz, *J. Appl. Phys.* **94**, 6477 (2003).

¹⁰D. M. Follstaedt, N. A. Missert, D. D. Koleske, C. C. Mitchell, and K. C. Cross, *Appl. Phys. Lett.* **83**, 4797 (2003).

¹¹B. Jahnen, M. Albrecht, W. Dorsch, S. Christiansen, H. P. Strunk, D. Hanser, and R. F. Davis, *MRS Internet J. Nitride Semicond. Res.* **3**, 39 (1998).

¹²R. Liu, J. Mei, S. Srinivasan, F. A. Ponce, H. Omiya, Y. Narukawa, and T. Mukai, *Appl. Phys. Lett.* **89**, 201911 (2006).

¹³Y. Cui and L. Li, *Phys. Rev. B* **66**, 155330 (2002).

¹⁴S. Ghosh, P. Waltereit, O. Brandt, H. T. Grahn, and K. H. Ploog, *Phys. Rev. B* **65**, 075202 (2002), and references therein.

¹⁵S. J. Henley and D. Cherns, *J. Appl. Phys.* **93**, 3934 (2003).

¹⁶See Ref. 15. For comparable excitation conditions, the authors estimated a decrease in the CL intensity of an (In,Ga)N/GaN single QW at the position of a TD of about 50% assuming that the dislocation acts as a perfect nonradiative sink for carriers.

¹⁷A. Hangleiter, F. Hitzel, C. Netzel, D. Fuhrmann, U. Rossow, G. Ade, and P. Hinze, *Phys. Rev. Lett.* **95**, 127402 (2005).